

Stability of ice lenses in saline soils

S. S. L. Peppin

Mississauga, L5G 2K5, Canada

(Received ?; revised ?; accepted ?.)

A model of the growth of an ice lens in a saline porous medium is developed. At high lens growth rates the pore fluid becomes supercooled relative to its equilibrium Clapeyron temperature. Instability occurs when the supercooling increases with distance away from the ice lens. Solute diffusion in the pore fluid significantly enhances the instability. An expression for the segregation potential of the soil is obtained from the condition for marginal stability of the ice lens. The model is applied to a clayey silt and a glass powder medium, indicating parameter regimes where the ice lens stability is controlled by viscous flow or by solute diffusion. A mushy layer, composed of vertical ice veins and horizontal ice lenses, forms in the soil in response to the instability. A marginal equilibrium condition is used to estimate the segregated ice fraction in the mushy layer as a function of the freezing rate and salinity.

Key words: frost heave, phase change, diffusion

1. Introduction

The freezing of soils and particulate suspensions has received increasing attention in recent years owing to its relevance to geophysical phenomena (Dash *et al.* 2006; Wettlaufer 2019), water purification (Gay & Azouni 2002; Gao *et al.* 2006) and materials science applications (Deville *et al.* 2006; Henderson *et al.* 2013; Deville 2017). In this process, ice is grown into a matrix of particles in water which may also contain dissolved salts and dispersants. For a range of freezing conditions and physical parameters, the ice segregates from the particle matrix, self-organizing into a variety of patterns (Taber 1929; Qian & Zhang 2011; Deville 2017). Materials scientists exploit this phenomenon to create novel microstructured and biomimetic materials (Deville 2013; Henderson *et al.* 2013). When soils freeze, the ice tends to segregate into a sequence of approximately planar horizontal layers called ice lenses (Taber 1929; Dash *et al.* 2006). While it is known that frost heave (the uplift of the soil surface in winter) is caused by the formation of ice lenses, the physical mechanisms governing their initiation and growth have yet to be fully explained (O'Neill 1983; Rempel 2010; Peppin & Style 2013; Wettlaufer 2019). In soils with a high clay content, ice lenses can become nonplanar, forming complex polygonal and reticulate vein structures (Taber 1929; Mackay 1974; Arenson *et al.* 2006; Peppin *et al.* 2006; Deville 2013; Wang *et al.* 2016; El Hasadi & Kodadadi 2015; Xu *et al.* 2016; You *et al.* 2018*b*). In addition, most soils and colloidal suspensions contain dissolved solutes in the pore fluid, which significantly influence the freezing process (Hallet 1978; Chamberlain 1983; Arenson *et al.* 2006; Pekor 2014; Wang *et al.* 2016; Schollick *et al.* 2016; You *et al.* 2018*a*; Ginot *et al.* 2019).

In the present work, a model of an ice lens growing in a saline porous medium is developed and a linear stability analysis is undertaken. A characteristic equation is obtained giving critical conditions for the onset of unstable lens growth, and a diagram is

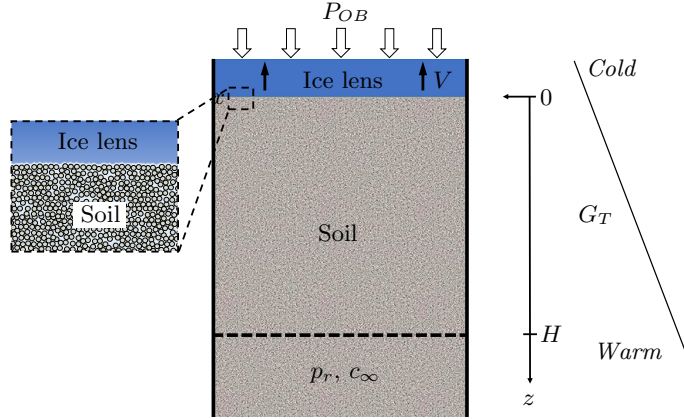


FIGURE 1. Schematic diagram of a directional solidification cell containing a saturated soil with an ice lens at $z = 0$ and a reservoir at $z = H$. The reservoir contains pore fluid at pressure p_r and solute concentration c_∞ . The ice lens is growing at speed V within a fixed temperature gradient G_T under an overburden pressure P_{OB} .

constructed illustrating parameter regimes in which molecular diffusion or viscous flow controls the instability. The diagram indicates that dissolved impurities have significant effects on the growth and stability of ice lenses at the solute concentrations typically found in soils and freeze-casting applications. The results are applied to frost heave experiments on a silty clay soil (Konrad 1990a) and a glass powder medium (Watanabe *et al.* 2001; Watanabe 2002).

2. Ice lens growth in saline porous media

The system to be studied, shown in figure 1, consists of a solidification cell containing a column of soil freezing from the top down. The soil is made up of solid particles, and the pore fluid is composed of water and a dissolved solute. At the soil surface $z = 0$ is a planar ice lens that is growing without entering the soil pores (primary frost heave); an overburden pressure P_{OB} acts on the top of the ice lens, so that the ice pressure is $p_i = P_{OB}$. Supplying the soil at position $z = H$ is a fluid reservoir at pressure p_r and solute concentration c_∞ . A linear temperature gradient is imposed on the system, and a constant freezing speed V . This can be achieved by ramping the temperatures at the top and base (Penner 1986; Konrad 1989a) or by moving the soil at speed V through a fixed temperature gradient (Watanabe & Mizoguchi 2000; Peppin *et al.* 2008; Anderson & Worster 2014; Schollick *et al.* 2016; You *et al.* 2018a; Saint-Michel *et al.* 2019). At steady state the ice lens growth speed V_{il} is equal to V .

2.1. Governing equations

In the following the density differences between ice, water, particles and solute are neglected. The equations describing the system can then be written, in a frame of reference moving with the freezing speed V , as

$$T = T_0 + G_T z \quad (z > 0), \quad (2.1)$$

$$\frac{\partial p}{\partial t} - V \frac{\partial p}{\partial z} = C_v \frac{\partial^2 p}{\partial z^2} \quad (0 < z < H) \quad (2.2)$$

$$\frac{\partial c}{\partial t} - V \frac{\partial c}{\partial z} = D \frac{\partial^2 c}{\partial z^2} \quad (0 < z < \infty), \quad (2.3)$$

where T_0 is the temperature at the ice lens surface $z = 0$, G_T is the temperature gradient, p is the Darcy pressure of the pore fluid, C_v is the consolidation coefficient of the soil, c is the solute concentration in the pore fluid and D is the solute diffusivity in the soil (Freeze & Cherry 1979; Wang 2000; Davis 2001; Bear 1972). Equation (2.2) is the pressure diffusion equation of consolidation theory written in a frame of reference moving with V (Appendix A). Typically $C_v \gg D$ for silt or clay soils (Bear 1972; Wang 2000).

The boundary conditions on (2.2) and (2.3) are

$$V = \frac{k}{\mu} \frac{\partial p}{\partial z}, \quad (c_0 - c_s)V = -D \frac{\partial c}{\partial z} \quad (z = 0), \quad (2.4)$$

$$p = p_r \quad (z = H) \quad \text{and} \quad c \rightarrow c_\infty \quad (z \rightarrow \infty), \quad (2.5)$$

where k is the soil permeability, μ is the fluid viscosity, c_0 is the solute concentration at the ice lens surface, $c_s = k_s c_0$ is the solute concentration in the ice lens and k_s is the solute segregation coefficient. For $k_s < 1$ the ice lens tends to push ahead solute molecules, forming a concentrated boundary layer adjacent to the ice surface (Hallet 1978; Chamberlain 1983; Konrad & McCammon 1990b; Watanabe *et al.* 2001; Wang *et al.* 2016). The thickness of the solute boundary layer, $D/V \sim 1\text{mm}$, is assumed much smaller than the soil height $H \sim 10\text{ cm}$.

2.2. Steady-state solution

At steady state, $c_s = c_\infty$ and equations (2.2)–(2.5) can be solved to give the pressure and solute profiles

$$p = p_0 + \frac{\mu C_v}{k} \left(1 - e^{-zV/C_v}\right) \quad (0 \leq z \leq H), \quad (2.6)$$

$$c = c_\infty + (c_0 - c_\infty)e^{-zV/D} \quad (z \geq 0). \quad (2.7)$$

where $p_0 = p_r - (\mu C_v/k)(1 - e^{-HV/C_v})$ and $c_0 = c_\infty/k_s$ are the pore pressure and concentration at the ice lens surface (Appendix B). In the case of a rigid porous matrix (Peppin 2009), $C_v \rightarrow \infty$ and the pressure profile is linear

$$p = p_r + \frac{\mu V}{k}(z - H) \quad (0 \leq z \leq H). \quad (2.8)$$

Equations (2.1), (2.6) and (2.7) are plotted on figure 2 for the case $V = 1\ \mu\text{m/s}$, $c_\infty = 0.1\ \text{g/L}$, $G_T = 20\ \text{K/m}$, $P_{OB} = 100\ \text{kPa}$, $H = 10\ \text{cm}$, with physical and clay soil parameters $\mu = .0015\ \text{Pa s}$, $C_v = 10^{-8}\ \text{m}^2/\text{s}$, $k = 10^{-16}\ \text{m}^2$, $D = 10^{-9}\ \text{m}^2/\text{s}$ and $k_s = 0.1$.

2.3. Ice lens temperature

The equilibrium freezing temperature T_{Cl} of the soil can be obtained from the generalized Clapeyron equation

$$\frac{L_f(T_{Cl} - T_m)}{T_m} = \nu_w(p - \pi) - \nu_i p_i, \quad (2.9)$$

where T_m is the melting temperature of pure ice at atmospheric pressure, ν_w/i is the specific volume of water/ice, L_f is the latent heat per unit mass of ice, p_i is the ice pressure (relative to atmospheric pressure), p is the pore fluid pressure (suction) and π is the solute osmotic pressure (O'Neill 1983; Acker *et al.* 2001; Peppin & Style 2013). Neglecting the density difference between water and ice ($\nu_i = \nu_w = 1/\rho$) and assuming

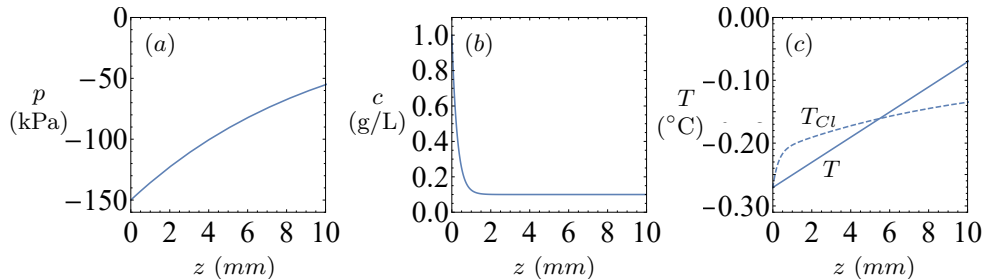


FIGURE 2. Steady-state (a) pore pressure, (b) solute concentration and (c) temperature profiles in the soil below the ice lens in figure 1, calculated from equations (2.1), (2.6), (2.7) and (2.11). The dashed curve in (c) is the Clapeyron temperature (2.10).

| T_m (K) | ρ (kg/m ³) | L_f (J/kg) | m (KL/g) | μ (Pas) | g (m ² /s) |
|-----------|-----------------------------|-------------------|------------|-------------|-------------------------|
| 273.15 | 1000 | 3.3×10^5 | 0.064 | 0.0015 | 9.81 |

TABLE 1. Physical parameters for water-ice near 0°C.

the solute is dilute, the Clapeyron equation (2.9) can be written as

$$T_{Cl} = T_m - \frac{T_m}{\rho L_f} (p_i - p) - mc, \quad (2.10)$$

where ρ is the density of water and $mc = T_m \pi / (\rho L_f)$. For dilute NaCl in water, $m = iK_f/M_w$ is the slope of the solute freezing temperature curve, where $i = 2$ is the Van't Hoff coefficient, $K_f = 1.86$ KL/mol is the molar cryoscopic constant (Schollick *et al.* 2016) and $M_w = 58.4$ g/mol is the NaCl molar mass. The other parameters used in equation (2.10) are $T_m = 273.15$ K, $\rho = 1000$ kg/m³ and $L_f = 3.3 \times 10^5$ J/kg (Table 1).

Assuming the ice lens pressure is equal to the overburden, $p_i = P_{OB}$, the temperature T_0 at the ice lens–soil boundary $z = 0$ can be obtained from (2.10) as

$$T_0 = T_m - \frac{T_m}{\rho L_f} (P_{OB} - p_0) - mc_0, \quad (2.11)$$

where p_0 and c_0 are the pore pressure and solute concentration at $z = 0$.

2.3.1. Constitutional and geometric supercooling

In solidification of aqueous solutions, constitutional supercooling of the solution adjacent to the ice interface occurs when $dT_L/dz > dT/dz$, where $T_L = T_m - mc$ is the freezing temperature (liquidus) of the solution and $dT/dz = G_T$ is the temperature gradient (Worster 1986; Davis 2001). Constitutional supercooling typically leads to instabilities because perturbations of the interface move into supercooled regions and experience accelerated growth (Tiller *et al.* 1953; Davis 2001).

Analogously, supercooling of the soil occurs when the gradient of the Clapeyron temperature is larger than the temperature gradient at the ice lens such that $dT_{Cl}/dz > dT/dz$, or with (2.10),

$$-m \frac{dc}{dz} + \frac{T_m}{\rho L_f} \frac{dp}{dz} > \frac{dT}{dz} \quad (z = 0). \quad (2.12)$$

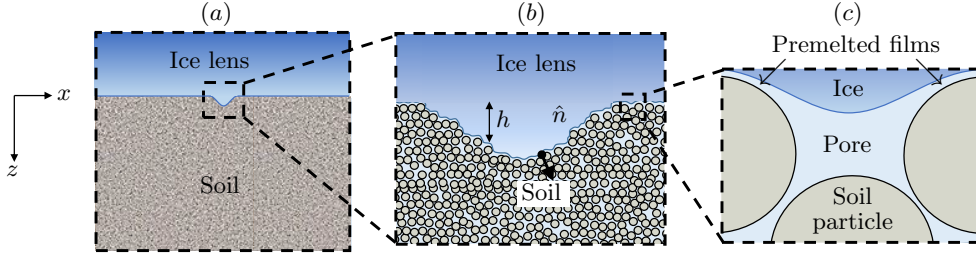


FIGURE 3. (a) Illustration of a macroscopic perturbation to the shape of the ice lens. If the perturbation continues to grow in size the ice lens is unstable; if all such perturbations melt back to the planar state the ice lens is stable. (b) The perturbed region is magnified, showing the height $h(x)$ and the unit normal \hat{n} . (c) Further magnification shows the premelted films and the ice curvature on the pore scale.

The first term on the left-hand-side of (2.12) accounts for constitutional supercooling caused by solute diffusion, while the second term accounts for geometric (hydraulic) supercooling caused by viscous flow (Rempel 2008; Style *et al.* 2011; You *et al.* 2018*b*). In terms of dimensionless parameters equation (2.12) can be written as

$$\mathcal{M}_c + \mathcal{M}_p > 1, \quad (2.13)$$

where $\mathcal{M}_c = -mG_c/G_T$ and $\mathcal{M}_p = T_m G_p / (\rho L_f G_T)$ are the solutal and hydraulic morphological numbers, respectively; $G_c = dc/dz|_{z=0} = -(c_0 - c_\infty)V/D$ and $G_p = dp/dz|_{z=0} = \mu V/k$ are the solute and pressure gradients at the ice lens interface. Figure 2c plots $T_{Cl}(z)$ and $T(z)$ for the pressure and solute profiles obtained in Section 2.2, showing a supercooled region below the ice lens.

3. Linear stability analysis

In linear stability analysis, the shape of the ice interface is perturbed, as in figure 3a, and the governing equations are linearized about the planar steady-state solution. If the perturbations tend to diminish back to the planar state the ice lens is stable, while it is unstable if perturbations tend to grow. Assuming the linear temperature profile imposed by the boundary conditions is stable and not perturbed (frozen temperature approximation (Davis 2001)), the governing equations describing the evolution of the perturbed ice lens are

$$T = T_0 + G_T z, \quad (3.1)$$

$$\frac{\partial p}{\partial t} - V \frac{\partial p}{\partial z} = C_v \nabla^2 p, \quad (3.2)$$

$$\frac{\partial c}{\partial t} - V \frac{\partial c}{\partial z} = D \nabla^2 c, \quad (3.3)$$

$$V_n = \frac{k}{\eta} \nabla p \cdot \hat{n}, \quad c(1 - k_s)V_n = -D \nabla c \cdot \hat{n} \quad (z = h), \quad (3.4)$$

$$T_h = T_m - mc_h - \frac{T_m}{\rho_l L_f} (P_{OB} - p_h) \quad (z = h), \quad (3.5)$$

where $h = h(x, t)$ is the height of the deformed interface and

$$\hat{n} = \frac{(-h_x, 1)}{\sqrt{1 + h_x^2}} \quad \text{and} \quad V_n = V \frac{(1 + h_t)}{\sqrt{1 + h_x^2}} \quad (3.6)$$

are, respectively, the unit normal \hat{n} to the ice lens surface and the ice velocity V_n along the normal direction (Mullins & Sekerka 1964; Davis 2001).

Latent heat and differing thermal conductivities have been neglected here, because many frost-heave experiments are designed to ensure that latent heat is quickly conducted away leading to linear temperature profiles (Watanabe & Mizoguchi 2000; Anderson & Worster 2014; Schollick 2015; Schollick *et al.* 2016; You *et al.* 2018a). The frozen temperature approximation also simplifies the analysis and allows the focus to be on the physical processes of diffusion and viscous flow that drive the ice lens instability. Accounting for latent heat effects leads to qualitatively similar results, with the thermal gradient G_T replaced by a weighted average \bar{G}_T of the gradients in the frozen and unfrozen regions (Mullins & Sekerka 1964; Sekerka 1968; Davis 2001).

Before linearizing the equations it is convenient to write them in dimensionless form. The solutions (2.6) and (2.7) suggest the scalings

$$(x^*, z^*) = \left(\frac{x}{\delta_l}, \frac{z}{\delta_t} \right), \quad t^* = \frac{t}{\delta_t}, \quad p^* = \frac{(p - p_0)}{\delta_l G_p}, \quad c^* = \frac{(c - c_0)}{\delta_l G_c}, \quad T^* = \frac{(T - T_0)}{\delta_l G_T},$$

where $\delta_l = D/V$ and $\delta_t = D/V^2$ are length and time scales, $G_p = \mu V/k$ is the steady-state Darcy pressure gradient at $z = 0$ and $G_c = -c_0 V(1 - k_s)/D$ is the steady-state solute gradient at $z = 0$. In dimensionless form the governing equations (3.1)–(3.3) become (upon dropping the stars)

$$T = z, \quad p_t - p_z = \epsilon_p \nabla^2 p, \quad c_t - c_z = \nabla^2 c, \quad (3.7)$$

where $\epsilon_p = C_v/D$ is the ratio of the soil consolidation coefficient to the solute diffusivity. The boundary conditions (3.4) and (3.5) become

$$\hat{V}_n = \nabla p \cdot \hat{n}, \quad [c(1 - k_s) + 1] \hat{V}_n = -\nabla c \cdot \hat{n} \quad (z = h), \quad (3.8)$$

$$T_h = \mathcal{M}_p p_h + \mathcal{M}_c c_h \quad (z = h), \quad (3.9)$$

where $\hat{V}_n = V_n/V$ and the dimensionless numbers

$$\mathcal{M}_p = \frac{T_m G_p}{\rho L_f G_T} \quad \text{and} \quad \mathcal{M}_c = -\frac{m G_c}{G_T} \quad (3.10)$$

are, respectively, the hydraulic and diffusive morphological numbers introduced in Section 2.3.1. The steady base-state solutions (2.7) and (2.8) become, in terms of dimensionless quantities,

$$\begin{bmatrix} c \\ p \\ h \end{bmatrix} = \begin{bmatrix} \bar{c} \\ \bar{p} \\ \bar{h} \end{bmatrix} = \begin{bmatrix} 1 - e^{-z} \\ \epsilon_p (1 - e^{-z/\epsilon_p}) \\ 0 \end{bmatrix} \quad (3.11)$$

Let the base state be perturbed such that

$$p = \bar{p} + p', \quad c = \bar{c} + c', \quad h = \bar{h} + h', \quad (3.12)$$

where the perturbations (p', c', h') take the form of normal modes

$$p' = p_1(z) e^{iqx + \omega t}, \quad c' = c_1(z) e^{iqx + \omega t}, \quad h' = h_1(z) e^{iqx + \omega t}. \quad (3.13)$$

Here q is the wave number and ω the growth rate of the perturbation (Mullins & Sekerka

1964; Davis 2001). If $\omega < 0$ for all wave numbers q , the perturbations decay in time and the ice lens is stable, while if $\omega > 0$ for any wave number the perturbation grows and the ice lens is unstable. In general the growth rate can also be a complex number, with the imaginary component describing oscillatory instabilities (Davis 2001). An imaginary component to ω can appear, for example, if the segregation coefficient k_s depends on the growth rate V (Coriell & Sekerka 1983; Davis 2001). In fact for lake ice k_s does depend on V (Weeks & Lofgren 1967), and experiments by Konrad & McCammon (1990b) suggest the same is true for ice lenses. Here, for simplicity, the segregation coefficient is treated as an averaged constant so that ω is real (Sekerka 1968; Wollkind & Segel 1970) and the interface experiences only transverse wave instabilities.

Inserting (3.12) and (3.13) into (3.7), linearizing in the primed quantities, and solving the resulting system of ordinary differential equations leads to the following expression for the growth rate ω (Appendix C)

$$\mathcal{M}_p + \mathcal{M}_c = 1 + \mathcal{M}_p \frac{(\omega + \epsilon_p^{-1})}{r_p} + \mathcal{M}_c \frac{(\omega + k_s)}{(k_s + r_c - 1)}, \quad (3.14)$$

where

$$r_p = \frac{1}{2}\epsilon_p^{-1} \left[1 + \sqrt{1 + 4\epsilon_p(\omega + \epsilon_p q^2)} \right] \quad \text{and} \quad r_c = \frac{1}{2} \left[1 + \sqrt{1 + 4(\omega + q^2)} \right].$$

Equation (3.14) is a nonlinear equation for ω that must in general be solved numerically. However, a simpler result can be obtained in the large wave number limit $q \gg 1$ (Mullins & Sekerka 1964; Davis 2001). In this case $r_p \approx r_c \approx q$ and, given that $\epsilon_p^{-1} = D/C_v < 1$ and $k_s < 1$, equation (3.14) becomes

$$\omega \approx q \left(1 - [\mathcal{M}_p + \mathcal{M}_c]^{-1} \right). \quad (3.15)$$

Equation (3.15) shows that ω is positive when $\mathcal{M}_p + \mathcal{M}_c > 1$, and therefore the supercooling condition (2.13) leads to instability. The dimensional wavelength of the instability is $\lambda = 2\pi D/qV$ so that, for a salt diffusivity $D \sim 10^{-9}\text{m}^2/\text{s}$ and ice lens growth rate $V \sim 1\mu\text{m}/\text{s}$, the condition $q \gg 1$ implies $\lambda \ll 1\text{cm}$. Given the minimum observable size of segregated ice is of order the particle radius $R \sim 1\mu\text{m}$, this suggests bounds on the initial wavelength of the form $1\mu\text{m} \ll \lambda \ll 1\text{cm}$.

Setting $\omega = 0$ in (3.15) gives the marginal stability condition

$$\mathcal{M}_p + \mathcal{M}_c = 1. \quad (3.16)$$

In terms of dimensional parameters the marginal stability condition (3.16) can be written as

$$\frac{T_m \mu V}{G_T \rho_l L_f k} + \frac{m c_\infty V (1 - k_s)}{D k_s G_T} = 1. \quad (3.17)$$

The first term on the left-hand side of (3.17) accounts for geometric (hydraulic) supercooling, while the second term accounts for constitutional supercooling. This equation will be used in Section 5 to study the stability of ice lenses in a clayey silt and a soil composed of glass microspheres. First, some implications of the instability are discussed in Section 4.

4. Mushy layers in freezing porous media

4.1. Instability and mushy layer growth

Morphological instability during the solidification of fluids leads to the formation of a mushy layer composed of vertical ice dendrites and interstitial fluid (Worster 1986). The

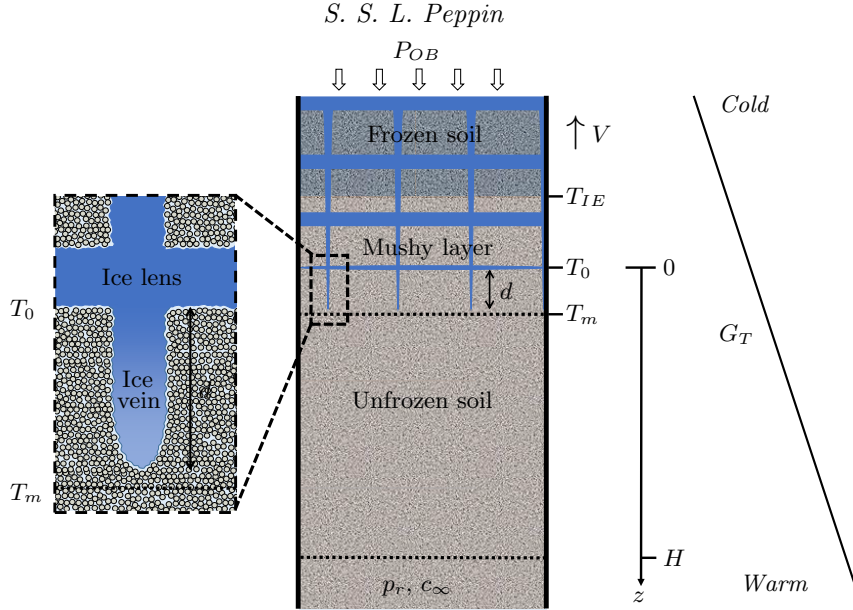


FIGURE 4. Schematic diagram of a mushy layer in a freezing saline soil. The mushy layer is composed of vertical ice veins and horizontal ice lenses. The portion of the mushy layer between the warmest ice lens at temperature T_0 and the freezing front near $T_m = 0^\circ\text{C}$ is the frozen fringe. T_{IE} is the temperature at which ice first enters the pore space. Here the system is experiencing primary frost heave ($T_{IE} < T_0$) and the soil surrounding the warmest ice lens is unfrozen. As in figure 1 there is a reservoir at $z = H$ containing pore fluid at pressure p_r and solute concentration c_∞ . The system is moving at steady freezing speed V within a fixed temperature gradient G_T under an overburden pressure P_{OB} , yielding a sequence of equally spaced ice lenses.

dendrites are a nonlinear manifestation of the planar instability and tend to form side branches in order to more efficiently remove the supercooling (Kurz & Fisher 1998; Davis 2001). Figure 4 illustrates a freezing soil in which a similar mushy layer has formed. The vertical ice veins in figure 4 are a nonlinear manifestation of the normal mode instability in Section 3. In three dimensions ice veins tend to form a polygonal pattern in the soil cross section (Taber 1929; Mackay 1974; Chamberlain & Gow 1979; Arenson *et al.* 2006, 2008; Wang *et al.* 2018). Assuming the analogy with alloy solidification holds also for the vein spacing, the primary spacing λ_1 can be estimated as

$$\lambda_1 = K_1 C_v^a V^{-a} G_T^{-b}, \quad (4.1)$$

where a , b and K_1 are positive constants (Kurz & Fisher 1998). Equation (4.1) indicates that the vein spacing decreases with the freezing speed V , and increases with the consolidation coefficient C_v , in qualitative agreement with the observations of Mackay (1974, 1975) and Chamberlain & Gow (1979). The horizontal ice lenses in figure 4 are assumed to nucleate as side branches from the vertical veins at the position of maximum supercooling (Style *et al.* 2011; You *et al.* 2018*a,b*). This ice-lens nucleation mechanism is in contrast to secondary frost heave in which horizontal ice lenses form in the absence of ice veins via a regelation-induced fracture of the frozen fringe (Miller 1978; Rempel *et al.* 2004; Style *et al.* 2011).

4.2. Primary and secondary frost heave

In figure 4 T_0 is the temperature of the warmest ice lens. The soil in between the ice lenses is unfrozen until the ice-entry temperature T_{IE} is reached and ice begins to enter

the pore space (Beskow 1935; Brown & Payne 1990). In soils with a uniform pore size distribution the ice-entry temperature is given by the Gibbs-Thompson equation, $T_{IE} = T_m(1 - 2\gamma/(R_p\rho L_f))$, where R_p is the pore size (Wettlaufer & Worster 2006; Peppin & Style 2013). Azmatch (2013) and Ginot *et al.* (2019) have shown that in soils with a broad size distribution or high salinity ice entry occurs over a finite range in temperature. In Miller's classification scheme (Miller 1972, 1978) figure 4 is an example of (unstable) *primary* frost heave, because the warmest ice lens is forming in the absence of pore ice ($T_0 > T_{IE}$). This is in contrast to *secondary* frost heave that occurs after ice has entered the pores ($T_0 < T_{IE}$).

Current research is ongoing to distinguish between primary and secondary frost heave, with some works finding evidence for ice lens formation in soil containing pore ice (Loch & Miller 1975; Konrad & Morgenstern 1982; Walder & Hallet 1986; Anderson & Worster 2012, 2014; Schollick *et al.* 2016; You *et al.* 2018*b*) and others finding ice lenses forming in soil regions that do not contain pore ice (Beskow 1935; Mackay 1975; Brown & Payne 1990; Watanabe *et al.* 1997; Watanabe & Mizoguchi 2000; You *et al.* 2018*a*). It may be that both types of frost heave can occur in the same system depending on the freezing conditions (Schollick 2015; You *et al.* 2018*b*). Microscale experiments capable of observing the pore contents during freezing, such as Raman spectroscopy (Watanabe & Mizoguchi 2000), X-ray scattering (Spannuth *et al.* 2011) and confocal microscopy (Saint-Michel *et al.* 2019; Ginot *et al.* 2019) will play an important role in clarifying the situation.

4.3. The frozen fringe

In the context of secondary frost heave, Miller (1972, 1978) defined the frozen fringe as the region between the warmest ice lens and the warmest extent of pore ice. Figure 4 suggests that a frozen fringe-like region can also be defined in the context of unstable primary frost heave as the region between the warmest ice lens and the warmest extent of segregated ice (tips of the ice veins). In the absence of solutes the ice veins extend very close to the 0 °C isotherm, in which case the primary frozen fringe has thickness $d \approx (T_m - T_0)/G_T$. In general, the frozen fringe can be defined as the region of soil between the warmest ice lens and the freezing front (warmest location of ice) (Konrad 1989*b*; Arenson *et al.* 2008).

4.3.1. Average permeability of the frozen fringe

In secondary frost heave the permeability k of the frozen fringe is reduced because of the presence of pore ice, which impedes the flow of water to the ice lens (Miller 1978; Konrad & Morgenstern 1981; Fowler & Krantz 1994; Rempel *et al.* 2004). In the unstable primary frost heave occurring in figure 4, the permeability of the frozen fringe region is also reduced because of consolidation of the soil between the ice veins, which reduces the pore size, and because of resistance to flow in premelted films at the ice lens–soil interface (Kuroda 1987; Worster & Wettlaufer 1999; Rempel 2008; Style & Peppin 2012; You *et al.* 2018*b*). Similarly to Konrad & Morgenstern (1980), the soil below the warmest ice lens can be modelled as a two-layer system with Darcy's law written as

$$V_{il} = \frac{p_r - p_0}{H\mu/k_u + d\mu/k}, \quad (4.2)$$

where V_{il} is the growth rate of the ice lens, k_u is the permeability of the unfrozen soil and k is the average permeability of the frozen fringe. In the case of no overburden pressure ($P_{OB} = p_r = 0$) and zero salinity ($c_0 = 0$), the Clapeyron equation (2.11) can

be combined with (4.2) to give

$$V_{il} = \frac{(L_f/gT_m)(T_m - T_0)}{H/K_u + d/K}, \quad (4.3)$$

where $K_u = \rho g k_u / \mu$ is the hydraulic conductivity of the unfrozen soil, $K = \rho g k / \mu$ is the hydraulic conductivity of the frozen fringe and g is the acceleration of gravity. By measuring the ice lens growth rate V_{il} , the ice lens temperature T_0 , the temperature gradient G_T , the unfrozen soil height H and hydraulic conductivity K_u , the frozen fringe thickness can be calculated as $d = (T_m - T_0)/G_T$, and equation (4.3) can be used to determine the frozen-fringe hydraulic conductivity K (Konrad & Morgenstern 1980).

5. Applications

5.1. Devon silt

Devon silt is a clayey silt soil with a broad particle size distribution that is highly frost-susceptible (Azmatch 2013). Konrad & Morgenstern (1980, 1981) measured the parameters in equation (4.3) for Devon silt at zero overburden and no salinity, and obtained a frozen fringe thickness $d \approx 1$ mm and hydraulic conductivity $K \approx 10^{-11}$ m/s. Konrad (1990a) also studied the effects of overburden pressure and salinity on ice lenses in Devon silt. The Clapeyron equation (2.11) shows that an overburden pressure P_{OB} moves the ice lens temperature T_0 to lower values. This has the effect of reducing the premelted film thicknesses and further reducing the permeability. Black (1990) reviewed various empirical equations that have been used to model the effect of an overburden pressure on the permeability of the frozen fringe. Here the Gardner equation is used in the form

$$K = K_0 e^{-\sigma/\sigma_K}, \quad (5.1)$$

where $\sigma = P_{OB} - p_0$ is the effective pressure on the soil matrix at $z = 0$, σ_K is a constant quantifying the effects of the overburden pressure on consolidation and flow in the premelted films, and K_0 is the hydraulic conductivity of the frozen fringe at zero effective pressure (Gilpin 1982; Konrad & Morgenstern 1984; Black 1990). An overburden pressure will also reduce the pore space available for solute diffusion, suggesting the diffusion coefficient be written as

$$D = D_0 e^{-\sigma/\sigma_D}, \quad (5.2)$$

where σ_D is a constant and D_0 is the diffusion coefficient of salt within the unstressed frozen fringe.

Azmatch (2013) measured the effective pressure $P_{OB} - p_0$ required for ice to enter the pores of Devon silt and found an ice-entry pressure of 175 kPa; the necessary pressure increased further when NaCl was added to the soil. The maximum overburden pressure in Konrad's experiments was $P_{OB} = 130$ kPa and the average pore pressure (suction) at the ice lens was $p_0 = -10$ kPa (Konrad 1990a), suggesting that the effective pressure was not sufficient for ice to enter the pores below the ice lens, at least in the high salinity experiments. Konrad (1990a) noted that "layers of unfrozen soil" may have been present between the ice lenses in his experiments because of the high salt concentrations. These results suggest that pore ice was not present in the frozen fringe of Konrad's experiments, and that the system was undergoing unstable primary frost heave.

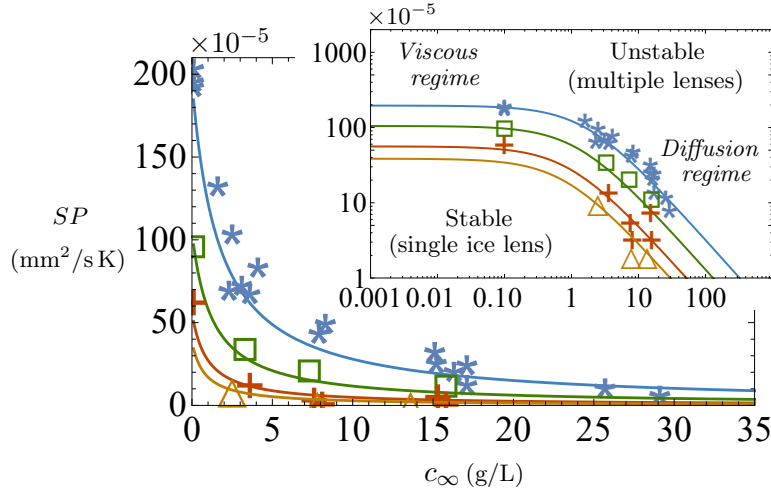


FIGURE 5. Plot of the segregation potential $SP = V_{il}/G_T$ versus salinity c_∞ for Devon silt; the data is from Konrad (1990a) at overburden pressures $P_{OB} = 0$ kPa (stars), 50 kPa (squares), 100 kPa (crosses) and 130 kPa (triangles) and average suction $p_0 = -10$ kPa. The leftmost data points correspond to the background salinity in the soil used in the experiments, estimated by Konrad (1990a) as $c_\infty = 0.1$ g/L. The curves are from equation (5.4). The inset plots the data on a log scale, showing a viscous regime at low c_∞ where $SP = L_f K/T_m g$, and a diffusion regime at high salinity where $SP = Dk_s/[mc_\infty(1 - k_s)]$.

5.1.1. The segregation potential

Konrad & Morgenstern (1980, 1981) introduced the segregation potential SP , defined as

$$SP = V_{il}/G_T, \quad (5.3)$$

where V_{il} and G_T are measurements of the ice lens growth rate and temperature gradient at the onset of the formation of the final ice lens during transient freezing. For sufficiently small freezing rates SP is a property of the soil, independent of the freezing parameters, and larger values of SP indicate a greater propensity of the soil to heave (Konrad & Morgenstern 1981; Konrad 1987). Konrad (1990a) measured the segregation potential of Devon silt over a range of overburden pressures and salinities, shown in figure 5 as a regime diagram for SP versus c_∞ . Assuming the onset of the final ice lens corresponds to a state of marginal stability such that $V_{il} = V$, the segregation potential can be obtained from equation (3.17) as

$$SP = \left(\frac{T_m g}{L_f K} + \frac{mc_\infty(1 - k_s)}{Dk_s} \right)^{-1}. \quad (5.4)$$

5.1.2. Regime diagram

The curves in figure 5 show SP versus c_∞ at several overburden pressures calculated from (5.4), using best-fit parameters $k_s = 0.2$, $K_0 = 1.8 \times 10^{-11}$ m/s, $\sigma_K = 80$ kPa, $D_0 = 10^{-9}$ m²/s and $\sigma_D = 55$ kPa (other parameters such as m and L_f are as given in Table 1). Below the curves the ice lens is predicted to grow stably (single ice lens), while above the curves it is unstable (mushy layer). There is a regime at low solute concentrations ($c_\infty < 0.1$ g/L) where the behaviour of the ice lens is independent of solute concentration, and the instability is caused by viscous flow through the soil layer and premelted films (geometric supercooling). In this regime the segregation potential (5.4)

takes the limiting value $SP = L_f K / T_m g$. At high solute concentrations the instability is owing mainly to solute diffusion (constitutional supercooling); the first term on the right-hand side of (5.4) becomes negligible in this regime and $SP = Dk_s / [mc_\infty(1 - k_s)]$. As the background solute concentrations in soils are typically above 0.1 g/L (Hivon & Segó 1993), these results suggest that frost heave often occurs in the diffusion regime, supporting the conclusions of Hallet (1978) and Chamberlain (1983) that solutes have significant effects on frost heave in periglacial soils.

The best-fit value for the hydraulic conductivity K_0 of the frozen fringe is similar to that measured by Konrad & Morgenstern (1980) (10^{-11} m/s). The best-fit value for the NaCl segregation coefficient k_s is similar to the measured value $k_s \approx 0.1$ for lake ice (Weeks & Lofgren 1967; Leppäranta 2015) but much larger than the equilibrium value ($k_s < 10^{-3}$) for pure ice crystals (Gross *et al.* 1987). However Konrad & McCammon (1990b) also found that k_s for Devon silt is larger than 0.1. Similarly Butler (2001) found, when freezing aqueous sucrose and polymer solutions, that a large segregation coefficient ($k_s > 0.1$) was needed in the Mullins-Sekerka equation to accurately model the instability.

A potential explanation for the relatively large segregation coefficient is the presence of grain boundaries and defects in the ice. Weeks & Lofgren (1967) show that lake ice is highly polycrystalline, in which case solute can be concentrated in between the grain boundaries (Thomson *et al.* 2013). Penner (1961) showed that ice lenses are also polycrystalline, and Wang *et al.* (2018) found that ice lenses contain significant defects that could also entrap salt. Furthermore, in soils such as Devon silt with a broad size distribution, salt could be transported in premelted films adjacent to the largest particles as they are engulfed by the ice during particle sorting (Corte 1962; Körber 1988). The ice–soil interface during lens growth is therefore a complex non-equilibrium system, with multiple mechanisms for solute entrapment, in contrast to the equilibrium ice–solution interface with a single ice grain used to obtain the much smaller equilibrium segregation coefficient (Gross *et al.* 1987).

5.2. Glass powder

Watanabe *et al.* (2001) and Watanabe (2002) performed a series of frost-heave experiments on a soil composed of glass microparticles. Figure 4 is a schematic of their system, in which a Hele-Shaw cell containing the water-saturated powder is moved at speed V through a temperature gradient G_T , yielding a sequence of equally-spaced ice lenses. Watanabe *et al.* (2001) varied the salinity c_∞ of the pore fluid and Watanabe (2002) varied the freezing speed V , and the effects on the ice lens thicknesses t_h and spacings s_p were measured.

5.2.1. Steady-state mushy layer

The system in figure 4 can be modelled as a mushy layer containing segregated ice of volume fraction Φ (Worster 1986; Peppin *et al.* 2007). Developing a full mushy layer model is beyond the scope of the present work; however, some results can be obtained by writing the boundary conditions at the position of the warmest ice lens $z = 0$ as

$$V_{il} = \frac{k}{\mu} \frac{dp}{dz} \quad \text{and} \quad (c_0 - c_s)V = -D \frac{dc}{dz} \quad (z = 0), \quad (5.5)$$

where

$$V_{il} = \Phi V \quad \text{and} \quad c_0 = \Phi c_s / k_s + (1 - \Phi)c_s, \quad (5.6)$$

are, respectively, the average growth speed V_{il} of the warmest ice lens and the average solute concentration c_0 at the ice lens. The first term in the expression for c_0 accounts for

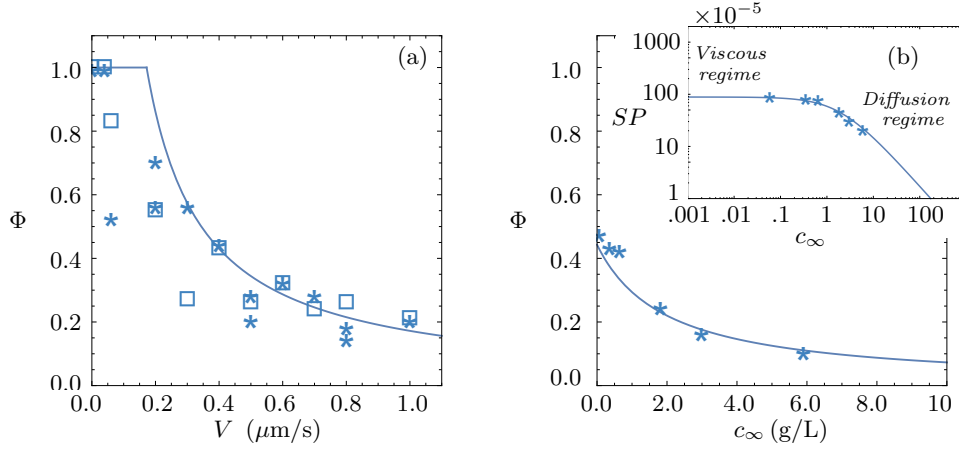


FIGURE 6. (a) Plot of segregated ice fraction Φ versus freezing rate V for the case $c_\infty = 0$ and $G_T = 190 \text{ K/m}$. The data, from Watanabe (2002), are from measurements of ice lens thicknesses t_h and spacings s_p , with the segregated ice fraction estimated as $\Phi = t_h/(s_p + t_h)$ (stars). Also shown is Φ data obtained from measurements of the ice lens growth rates V_{il} using $\Phi = V_{il}/V$ (squares). The curve is from equation (5.9). Below $V = 0.19 \mu\text{m/s}$ the ice lens is predicted to be stable ($\Phi = 1$). (b) Plot of Φ versus the salinity c_∞ for the case $V = 0.4 \mu\text{m/s}$ and $G_T = 210 \text{ K/m}$. The Φ data (stars) are from ice lens thickness and spacing measurements (Watanabe *et al.* 2001). The leftmost data point corresponds to the background salinity in the soil, estimated from Watanabe *et al.* (2001) as $c_\infty \approx 0.001 \text{ M} = 0.06 \text{ g/L}$. The inset shows the segregation potential calculated as $SP = V_{il}/G_T$. The curves are from equations (5.9) and (5.10).

the solute rejected by the warmest ice lens, while the second term accounts for the solute trapped in between the ice lenses. When $\Phi = 1$ (single stable ice lens), $c_0 = c_\infty/k_s$ as in Section 2.2. At steady state $c_s = c_\infty$ is the average solute concentration in the mushy layer.

Assuming that segregated ice forms to eliminate supercooling and return the system to local equilibrium (Worster 1986), the temperature everywhere in the mushy layer is given by the Clapeyron equation (2.10). In the experiments of Watanabe *et al.* (2001) the overburden and reservoir pressures were equal to atmospheric pressure so that $P_{OB} = p_i = p_r = 0$ and (2.10) becomes

$$T_{Cl} = T_m + \frac{T_m}{\rho L_f} p - mc. \quad (5.7)$$

Following Worster (1986), the segregated ice fraction Φ in the mushy layer can be obtained by assuming marginal equilibrium in the mushy layer so that

$$\frac{dT}{dz} = \frac{dT_{Cl}}{dz} \quad (z = 0), \quad (5.8)$$

or, with (5.5)–(5.7),

$$\Phi = \frac{G_T}{V} \left(\frac{T_m g}{L_f K} + \frac{mc_\infty(1 - k_s)}{k_s D} \right)^{-1}, \quad (5.9)$$

where $K = k\rho g/\mu$ is the hydraulic conductivity of the frozen fringe. To determine K from the Gardner equation (5.1) it is necessary to solve the full mushy layer model to calculate

the pore pressure p and effective pressure $\sigma = P_{OB} - p$ profiles. However, since Watanabe (2002) did not use an overburden pressure, and used a small freezing cell ($H \sim 5$ cm), it can be assumed that $\sigma \ll \sigma_K$, and treat K and D as averaged constants.

Figure 6 shows Φ vs the freezing speed V and salinity c_∞ calculated from (5.9), along with experimental data from Watanabe *et al.* (2001) and Watanabe (2002), with best-fit parameters $k_s = 0.1$, $K = 0.7 \times 10^{-11}$ m/s and $D = 10^{-9}$ m²/s. The best-fit hydraulic conductivity K of the frozen fringe is similar to that for Devon silt (Konrad & Morgenstern 1980), while the NaCl segregation coefficient k_s is similar to that for lake ice (Leppäranta 2015). Also shown as the inset to figure 6 is the segregation potential estimated as

$$SP = \frac{V_{il}}{G_T} = \left(\frac{T_m g}{L_f K} + \frac{m c_\infty (1 - k_s)}{k_s D} \right)^{-1}. \quad (5.10)$$

Similarly to the case of Devon silt, the SP diagram shows a viscous regime at low salinity and a diffusion regime at high salinity. The magnitude of the segregation potential is less than the zero-overburden SP data in figure 5, indicating that the glass powder is somewhat less frost susceptible than Devon silt.

6. Conclusions

A model of the growth of an ice lens during primary frost heave in a saline soil has been developed, and a linear stability analysis undertaken, showing that a planar ice lens can become unstable because of supercooling. The characteristic equation for the marginal stability of the ice lens is related to the segregation potential of the soil. Segregation potential diagrams have been obtained for Devon silt and a glass powder medium, showing two distinct regimes: At low salinity the ice lens growth rate and stability is affected mainly by viscous flow in the soil and premelted films, while at high salinity it is controlled by salt diffusion. At unstable freezing rates a mushy layer, composed of a reticulate network of ice lenses and vertical ice veins, forms in order to remove the supercooling. A mushy layer model has been used to determine the segregated ice fraction in the mushy layer as a function of the salinity and freezing rate.

Discussions with D. G. A. L. Aarts, A. M. Anderson, S. Deville, J. A. W. Elliott, A. C. Fowler, P. Guba, M. G. Hennessey, R. F. Katz, F. Lampl, C. B. Macdonald, A. Majumdar, M. D. Patterson, G. C. Sander, J. M. H. Schollick, D. C. Sego, M. Spannuth, R. W. Style, E. S. Thomson, J. S. Wettlaufer, L. A. Wilen, P. J. Williams and M. G. Worster are gratefully acknowledged, as are helpful comments from the referees. I thank Ontario Works and my family for financial support. *All things were made by Him; and without Him was not any thing made that was made.* John 1:3

Declaration of Interests. The author reports no conflict of interest.

Appendix A

Assuming the porous medium is composed of inert incompressible particles and an incompressible fluid, conservation of mass can be written as

$$\frac{\partial \phi}{\partial t} + \nabla \cdot \phi \mathbf{v}_p = 0 \quad \text{and} \quad \nabla \cdot \mathbf{v} = 0, \quad (\text{A } 1)$$

where ϕ is the volume fraction of solids in a representative volume element, $1 - \phi$ is the porosity, \mathbf{v}_p is the average velocity of the porous matrix, $\mathbf{v} = \phi \mathbf{v}_p + (1 - \phi) \mathbf{v}_f$ is the

volume average velocity of the mixture and \mathbf{v}_f is the average fluid velocity (deGroot & Mazur 1962; Bear 1972). Using the identity $\nabla \cdot \phi \mathbf{v} = \phi \nabla \cdot \mathbf{v} + \mathbf{v} \cdot \nabla \phi$ equations (A 1) can be combined to give

$$\frac{\partial \phi}{\partial t} + \mathbf{v} \cdot \nabla \phi = \nabla \cdot \phi \mathbf{q}, \quad (\text{A } 2)$$

where $\mathbf{q} = (\mathbf{v} - \mathbf{v}_p) = (1 - \phi)(\mathbf{v}_f - \mathbf{v}_p)$ is the volume velocity of the fluid relative to the porous matrix. Darcy's law can be written in the form

$$\mathbf{q} = -\frac{k}{\mu} \nabla p, \quad (\text{A } 3)$$

where p is the pore pressure (Bear 1972; Bear & Corapcioglu 1981). Assuming the constitutive relation $p = p(T, P, \phi)$, differentiating at constant temperature T and constant isotropic total pressure P gives

$$dp = -\Pi_\phi d\phi, \quad (\text{A } 4)$$

where $\Pi \equiv P - p$ is the effective pressure on the porous matrix and $\Pi_\phi = (\partial \Pi / \partial \phi)_{T, P}$. Combining (A 4) and (A 3) with (A 2) and assuming $\phi k / \mu$ is constant gives the pressure diffusion equation

$$\frac{\partial p}{\partial t} + \mathbf{v} \cdot \nabla p = C_v \nabla \cdot \nabla p, \quad (\text{A } 5)$$

where $C_v = \phi \frac{k}{\mu} \Pi_\phi$ is the consolidation coefficient. Finally, considering a one-dimensional system with $\mathbf{v} = -V \hat{z}$ gives equation (2.2).

Appendix B

At steady state $\partial p / \partial t = \partial c / \partial t = 0$ and equations (2.2) and (2.3) become

$$C_v \frac{d^2 p}{dz^2} + V \frac{dp}{dz} = 0, \quad D \frac{d^2 c}{dz^2} + V \frac{dc}{dz} = 0, \quad (\text{B } 1)$$

subject to the boundary conditions

$$V = \frac{k}{\mu} \frac{dp}{dz}, \quad (c_0 - c_s)V = -D \frac{dc}{dz} \quad (z = 0), \quad (\text{B } 2)$$

and

$$p = p_r \quad (z = H) \quad \text{and} \quad c \rightarrow c_\infty \quad (z \rightarrow \infty), \quad (\text{B } 3)$$

where $c_s = c_\infty$ and $c_0 = c_\infty / k_s$. The general solutions to (B 1) are of the form

$$p = A_p + B_p e^{r_p z} \quad \text{and} \quad c = A_c + B_c e^{r_c z}, \quad (\text{B } 4)$$

where $A_{p,c}, B_{p,c}, r_{p,c}$ are constants. Inserting (B 4) into (B 1) gives $r_p = -V/C_v$ and $r_c = -V/D$; inserting (B 4) into (B 2) gives $B_p = -C_v \mu / k$ and $B_c = c_0 - c_\infty$; equations (B 3) then require $A_p = p_r + (C_v \mu / k) e^{-VH/C_v}$ and $A_c = c_\infty$, giving (2.6) and (2.7).

Appendix C

Inserting (3.12) into (3.7) and linearizing in the primed quantities gives, bearing in mind that for the steady base state $\bar{c}_z + \bar{c}_{zz} = 0$ and $\bar{p}_z + \epsilon_p \bar{p}_{zz} = 0$,

$$p'_t - p'_z = \epsilon_p \nabla^2 p', \quad (\text{C } 1)$$

$$c'_t - c'_z = \nabla^2 c'. \quad (\text{C } 2)$$

The boundary conditions at the perturbed ice interface $z = h$ can be expanded via Taylor series about $z = 0$ (Davis 2001). To first order and neglecting terms nonlinear in primed quantities, bearing in mind that $\bar{c}(0) = 0$ and $\bar{c}_z(0) = 1$,

$$c(h) \approx c(0) + hc_z(0) = [\bar{c}(0) + c'(0)] + h[\bar{c}_z(0) + c'_z(0)] \approx h' + c'(0).$$

Similarly,

$$c_z(h) \approx 1 - h + c'_z(0), \quad p(h) \approx h' + p'(0) \quad \text{and} \quad p_z(h) \approx 1 - h'\epsilon_p^{-1} + p'_z(0).$$

Inserting these expansions into (3.8) gives, upon neglecting terms nonlinear in the primed quantities and using the linearized quantities $\hat{n} \approx (-h'_x, 1)$ and $V_n \approx V(1 + h'_t)$,

$$p'_z = h'\epsilon_p^{-1} + h'_t \quad \text{and} \quad c'_z = c'(1 - k_s) + h'k_s + h'_t \quad (z = 0). \quad (\text{C } 3)$$

Combining equations (3.7) and (3.9) at $z = h'$ and expanding about $z = 0$ gives

$$h' = \mathcal{M}_p(h' + p') + \mathcal{M}_c(h' + c') \quad (z = 0). \quad (\text{C } 4)$$

Inserting (p', c', h') from (3.13) into (C 1) and (C 2), and neglecting terms nonlinear in the perturbations, leads to the ordinary differential equations

$$\epsilon_p \frac{d^2 p_1}{dz^2} + \frac{dp_1}{dz} - (\omega + \epsilon_p q^2) p_1 = 0 \quad (z > 0), \quad (\text{C } 5)$$

$$\frac{d^2 c_1}{dz^2} + \frac{dc_1}{dz} - (\omega + q^2) c_1 = 0 \quad (z > 0). \quad (\text{C } 6)$$

With (3.13) the boundary conditions (C 3) become

$$\frac{dp_1}{dz} = (\epsilon_p^{-1} + \omega) h_1, \quad \frac{dc_1}{dz} = c_1(k_s - 1) + (k_s + \omega) h_1 \quad (z = 0), \quad (\text{C } 7)$$

and (C 4) gives

$$h_1 = \frac{\mathcal{M}_p p_1 + \mathcal{M}_c c_1}{1 - (\mathcal{M}_p + \mathcal{M}_c)}. \quad (\text{C } 8)$$

Assuming the perturbations decay far from the ice lens, the far-field boundary conditions are

$$p_1 \rightarrow 0, \quad c_1 \rightarrow 0 \quad (z \rightarrow \infty). \quad (\text{C } 9)$$

The solutions to (C 5) and (C 6) subject to (C 9) are

$$p_1 = Ae^{-r_p z}, \quad c_1 = Be^{-r_c z}, \quad (\text{C } 10)$$

where A and B are constants,

$$r_p = \frac{1}{2} \epsilon_p^{-1} \left[1 + \sqrt{1 + 4\epsilon_p(\omega + \epsilon_p q^2)} \right] \quad \text{and} \quad r_c = \frac{1}{2} \left[1 + \sqrt{1 + 4(\omega + q^2)} \right].$$

Eliminating h_1 between equations (C 7) and (C 8), and inserting the solutions (C 10) into the result, leads to the characteristic equation (3.14).

REFERENCES

- ACKER, J.P., ELLIOTT, J.A.W. & MCGANN, L. E. 2001 Intercellular ice propagation: Experimental evidence for ice growth through membrane pores. *Biophysical Journal* **81** (3), 1389–1397.
- ANDERSON, A. M. & WORSTER, M. G. 2012 Periodic ice banding in freezing colloidal dispersions. *Langmuir* **28**, 16512–16523.

- ANDERSON, A. M. & WORSTER, M. G. 2014 Freezing colloidal suspensions: Periodic ice lenses and compaction. *Journal of Fluid Mechanics* **758**, 786–808.
- ARENSEN, L. U., AZMATCH, T. F. & SEGO, D. C. 2008 A new hypothesis on ice lens formation in frost-susceptible soils. In *9th International Conference on Permafrost*, pp. 59–64. Fairbanks, Alaska.
- ARENSEN, L. U., XIA, D., SEGO, D. C. & BIGGAR, K. W. 2006 Change in ice lens formation for saline and non-saline Devon silt as a function of temperature and pressure. In *Cold Regions Engineering 2006: Current Practices in Cold Regions Engineering*, pp. 1–11.
- AZMATCH, T. F. 2013 Frost heave: New ice lens initiation condition and hydraulic conductivity prediction. PhD thesis, University of Alberta, Edmonton, Canada.
- BEAR, J. 1972 *Dynamics of Fluids in Porous Media*. NY: Elsevier.
- BEAR, JACOB & CORAPCIOGLU, M. YAVUZ 1981 Mathematical model for regional land subsidence due to pumping: 1. Integrated aquifer subsidence equations based on vertical displacement only. *Water Resources Research* **17** (4), 937–946.
- BESKOW, G. 1935 *Soil Freezing and Frost Heaving with Special Applications to Roads and Railroads*. Northwestern University: Technological Institute, reprinted in *Historical Perspectives in Frost Heave Research* (P. B. Black and M. J. Hardenberg, eds.) CRREL Special Report No. 91-23, pp 37–157, 1991.
- BLACK, P. 1990 Three functions that model empirically measured unfrozen water content and predict relative hydraulic conductivity. *CRREL Tech. Rep.* **90-5**, 1–7.
- BROWN, S. C. & PAYNE, D. 1990 Frost action in clay soils. II. Ice and water location and suction of unfrozen water in clays below 0 °C. *J. Soil Sci.* **41**, 547–561.
- BUTLER, MICHAEL F. 2001 Instability formation and directional dendritic growth of ice studied by optical interferometry. *Crystal Growth & Design* **1** (3), 213–223.
- CHAMBERLAIN, E. J. 1983 Frost heave of saline soils. In *Proceedings of the 4th International Conference on Permafrost*, pp. 121–126. Fairbanks, Alaska.
- CHAMBERLAIN, E. J. & GOW, A. J. 1979 Effect of freezing and thawing on the permeability and structure of soils. *Engineering Geology* **13**, 73–92.
- CORIELL, S. R. & SEKERKA, R. F. 1983 Oscillatory morphological instabilities due to nonequilibrium segregation. *Journal of Crystal Growth* **61**, 499–508.
- CORTE, A. E. 1962 Vertical migration of particles in front of a moving freezing plane. *Journal of Geophysical Research* **67** (3), 1085–1090.
- DASH, J. G., REMPEL, A. W. & WETTLAUER, J. S. 2006 The physics of premelted ice and its geophysical consequences. *Rev. Mod. Phys.* **78**, 695–741.
- DAVIS, S. H. 2001 *Theory of Solidification*. UK: Cambridge University Press.
- DEGROOT, S. R. & MAZUR, P. 1962 *Non-Equilibrium Thermodynamics*. Amsterdam: North-Holland Publishing Co.
- DEVILLE, S. 2013 Ice templating, freeze casting: Beyond materials processing. *J. Mater. Res.* **28**, 2202–2219.
- DEVILLE, S. 2017 *Freezing Colloids: Observations, Principles, Control, and Use*. Springer International.
- DEVILLE, S., SAIZ, E., NALLA, R. K. & TOMSIA, A. P. 2006 Freezing as a path to build complex composites. *Science* **311**, 515–518.
- EL HASADI, Y. M. F. & KODADADI, J. M. 2015 Numerical simulation of solidification of colloids inside a differentially heated cavity. *Journal of Heat Transfer* **137**, 072301.
- FOWLER, A. & KRANTZ, W. B. 1994 A generalized secondary frost heave model. *SIAM Journal on Applied Mathematics* **54**, 1650–1675.
- FREEZE, R. ALLAN & CHERRY, JOHN A. 1979 *Groundwater*. Upper Saddle River, NJ 07458: Prentice Hall, Inc.
- GAO, W., SMITH, D.W. & LI, Y. 2006 Natural freezing as a wastewater treatment method: E. coli inactivation capacity. *Water Research* **40** (12), 2321–2326.
- GAY, G. & AZOUNI, A. M. 2002 Forced migration of nonsoluble and soluble metallic pollutants ahead of a liquid-solid interface during unidirectional freezing of dilute clayey suspensions. *Cryst. Growth Des.* **2**, 135–140.
- GILPIN, R. R. 1982 A frost heave interface condition for use in numerical modelling. In *Engineering Applications in Permafrost Areas. Proceedings of the Fourth Canadian Permafrost Conference*, pp. 459–465.

- GINOT, F., LENAUVETIER, T., DEDOVETS, D. & DEVILLE, S. 2019 Solute effects in confined freezing. *arXiv e-prints* p. arXiv:1907.10502.
- GROSS, G. W., GUTJAHR, A. & CAYLOR, K. 1987 Recent experimental work on solute redistribution at the ice/water interface. Implications for electrical properties and interface processes. *J. Phys. Colloques* **48**, C1-527-533.
- HALLET, B. 1978 Solute redistribution in freezing ground. In *Proceedings of the 3rd International Conference on Permafrost*, pp. 86-91. Edmonton, Canada.
- HENDERSON, T.M.A., LADEWIQ, K., HAYLOCK, D.N., MACLEAN, K.M. & O'CONNOR, A.J. 2013 Cryogels for biomedical applications. *Journal of Materials Chemistry B* **1**, 2682-2695.
- HIVON, E.G. & SEGO, D.C. 1993 Distribution of saline permafrost in the Northwest Territories, Canada. *Canadian Geotechnical Journal* **30** (3), 506-514.
- KONRAD, J. M. 1987 Procedure for determining the segregation potential of freezing soils. *Geotechnical Testing Journal* **10**, 51-58.
- KONRAD, J.-M. 1989a Influence of cooling rate on the temperature of ice lens formation in clayey silts. *Cold Regions Science and Technology* **16** (1), 25 - 36.
- KONRAD, J.-M. 1989b Physical processes during freeze-thaw cycles in clayey silts. *Cold Regions Science and Technology* **16** (3), 291 - 303.
- KONRAD, J.-M. 1990a Segregation potential - pressure - salinity relationships near thermal steady state for a clayey silt. *Canadian Geotechnical Journal* **27** (2), 203-215.
- KONRAD, J.-M. & MCCAMMON, A. W. 1990b Solute partitioning in freezing soils. *Canadian Geotechnical Journal* **27** (6), 726-736.
- KONRAD, JEAN-MARIE & MORGENSTERN, NORBERT R. 1980 A mechanistic theory of ice lens formation in fine-grained soils. *Canadian Geotechnical Journal* **17** (4), 473-486.
- KONRAD, J. M. & MORGENSTERN, N. R. 1981 The segregation potential of a freezing soil. *Canadian Geotechnical Journal* **18**, 482-491.
- KONRAD, J.-M. & MORGENSTERN, N. R. 1982 Effects of applied pressure on freezing soils. *Canadian Geotechnical Journal* **19** (4), 494-505.
- KONRAD, J.-M. & MORGENSTERN, N. R. 1984 Frost heave prediction of chilled pipelines buried in unfrozen soils. *Canadian Geotechnical Journal* **21** (1), 100-115.
- KÖRBER, CHRISTOPH 1988 Phenomena at the advancing ice-liquid interface: solutes, particles and biological cells. *Quarterly Reviews of Biophysics* **21** (2), 229-298.
- KURODA, T. 1987 Role of water layer at an ice surface in the kinetic processes of growth of ice crystals - Growth of snow crystals and frost heaving. *Journal de Physique Colloques* **48** (C1), 487-493.
- KURZ, W. & FISHER, D. J. 1998 *Fundamentals of Solidification. Fourth Edition*. Zurich, Switzerland: Trans Tech Publications Ltd.
- LEPPÄRANTA, M. 2015 *Freezing of Lakes and the Evolution of Their Ice Cover*. Berlin: Springer-Verlag.
- LOCH, J.P.G. & MILLER, R. D. 1975 Tests of the concept of secondary heaving. *Soil Science Society of America Proceedings* **39**, 1036-1041.
- MACKAY, J. ROSS 1974 Reticulate ice veins in permafrost, northern Canada. *Canadian Geotechnical Journal* **11** (2), 230-237.
- MACKAY, J. ROSS 1975 Reticulate ice veins in permafrost, northern Canada: Reply. *Canadian Geotechnical Journal* **12**, 163-165.
- MILLER, R.D. 1972 Freezing and heaving of saturated and unsaturated soils. *Highway Research Record* **393**, 1-11.
- MILLER, R. D. 1978 Frost heaving in non-colloidal soils. *Proc. 3rd Inter. Conf. Permafrost, Edmonton, Alberta* pp. 708-713.
- MULLINS, W. W. & SEKERKA, R. F. 1964 Stability of a planar interface during solidification of a dilute binary alloy. *J. Appl. Phys.* **35**, 444-451.
- O'NEILL, K. 1983 The physics of mathematical frost heave models: A review. *Cold Regions Science and Technology* **6** (3), 275 - 291.
- PEKOR, C. M. 2014 The effect of the molecular weight of polyethylene glycol on the microstructure of freeze-cast alumina. *Ceram. Int.* **40**, 9171-9177.
- PENNER, E 1961 Ice-grain structure and crystal orientation in an ice lens from Leda clay. *Geological Society of America Bulletin* **72**, 1575-1577.

- PENNER, E. 1986 Aspects of ice lens growth in soils. *Cold Regions Science and Technology* **13** (1), 91–100.
- PEPPIN, S. S. L. 2009 On diffusion and permeation. *Journal of Non-Equilibrium Thermodynamics* **34**, 355–369.
- PEPPIN, S. S. L., AUSSILLOUS, P., HUPPERT, H. E. & WORSTER, M. G. 2007 Steady-state mushy layers: experiments and theory. *J. Fluid Mech.* **570**, 69–77.
- PEPPIN, S. S. L., ELLIOTT, J. A. W. & WORSTER, M. G. 2006 Solidification of colloidal suspensions. *J. Fluid Mech.* **554**, 147–166.
- PEPPIN, S. S. L. & STYLE, R. W. 2013 The physics of frost heave and ice-lens growth. *Vad. Zone J.* **12**.
- PEPPIN, S. S. L., WETTTLAUFER, J. S. & WORSTER, M. G. 2008 Experimental verification of morphological instability in freezing aqueous colloidal suspensions. *Phys. Rev. Lett.* **100**, 238301.
- QIAN, L. & ZHANG, H. 2011 Controlled freezing and freeze-drying: a versatile route for porous and micro-/nano-structured materials. *J. Chem. Technol. Biotechnol.* **86**, 172–184.
- REMPEL, A. W. 2008 A theory for ice-till interactions and sediment entrainment beneath glaciers. *Journal of Geophysical Research: Earth Surface* **113** (F1), 1–20.
- REMPEL, A. W. 2010 Frost heave. *J. Glaciol.* **56**, 1122–1128.
- REMPEL, A. W., WETTTLAUFER, J. S. & WORSTER, M. G. 2004 Premelting dynamics in a continuum model of frost heave. *J. Fluid Mech.* **498**, 227–244.
- SAINT-MICHEL, B., GEORGELIN, M., DEVILLE, S. & POCHEAU, A. 2019 Boundary-induced inhomogeneity of particle layers in the solidification of suspensions. *Phys. Rev. E* **99**, 052601.
- SCHOLLIK, J.M.H., STYLE, R.W., CURRAN, A., WETTTLAUFER, J. S., DUFRESNE, E.R., WARREN, P.B., VELIKOV, K.P., DULLENS, R.P.A. & AARTS, D.G.A.L. 2016 Segregated ice growth in a suspension of colloidal particles. *J. Phys. Chem. B* **120**, 3941–3949.
- SCHOLLIK, J. M. H. 2015 Real space study of pattern formation in freezing colloidal suspensions. PhD thesis, University of Oxford, Oxford, UK.
- SEKERKA, R.F. 1968 Morphological stability. *Journal of Crystal Growth* **3-4**, 71–81.
- SPANNUTH, M., MOCHRIE, S. G. J., PEPPIN, S. S. L. & WETTTLAUFER, J. S. 2011 Particle-scale structure in frozen colloidal suspensions from small-angle x-ray scattering. *Phys. Rev. E* **83**, 021402.
- STYLE, R. W. & PEPPIN, S. S. L. 2012 The kinetics of ice-lens growth in porous media. *J. Fluid Mech.* **692**, 482–498.
- STYLE, R. W., PEPPIN, S. S. L., COCKS, A. C. F. & WETTTLAUFER, J. S. 2011 Ice lens formation and geometrical supercooling in soils and other colloidal materials. *Phys. Rev. E* **84**, 041402.
- TABER, S. 1929 Frost heaving. *J. Geol.* **37**, 428–461.
- THOMSON, E. S., HANSEN-GOOS, H., WETTTLAUFER, J. S. & WILEN, L. A. 2013 Grain boundary melting in ice. *Journal of Chemical Physics* **138** (12), 124707.
- TILLER, W.A., JACKSON, K.A., RUTTER, J.W. & CHALMERS, B. 1953 The redistribution of solute atoms during the solidification of metals. *Acta Metallurgica* **1** (4), 428–437.
- WALDER, J. & HALLET, B. 1986 The physical basis of frost weathering: Toward a fundamental and unified perspective. *Arctic Alpine Res.* **18**, 27–32.
- WANG, H. 2000 *Theory of Linear Poroelasticity*. USA: Princeton University Press.
- WANG, L., YOU, J., WANG, Z., WANG, J. & LIN, X. 2016 Interface instability modes in freezing colloidal suspensions: revealed from onset of planar instability. *Scientific Reports* **6**, 23358.
- WANG, Y., WANG, D., MA, W., WEN, Z., CHEN, S. & XU, X. 2018 Laboratory observation and analysis of frost heave progression in clay from the Qinghai-Tibet Plateau. *Applied Thermal Engineering* **131**, 381–389.
- WATANABE, KUNIO 2002 Relationship between growth rate and supercooling in the formation of ice lenses in a glass powder. *Journal of Crystal Growth* **237-239**, 2194–2198.
- WATANABE, K. & MIZOGUCHI, M. 2000 Ice configuration near a growing ice lens in a freezing porous medium consisting of micro glass particles. *J. Cryst. Growth* **213**, 135–140.
- WATANABE, K., MIZOGUCHI, M., ISHIZAKI, T. & FUKUDA, M. 1997 Experimental study on microstructure near freezing front during soil freezing. In *Ground Freezing 97* (ed. S. Knutsson), pp. 187–192. Balkema, Rotterdam: CRC Press.
- WATANABE, K., MUTO, Y. & MIZOGUCHI, M. 2001 Water and solute distributions near an ice

- lens in a glass-powder medium saturated with sodium chloride solution under unidirectional freezing. *Crystal Growth & Design* **1** (3), 207–211.
- WEEKS, W. F. & LOFGREN, G. 1967 The effective solute distribution coefficient during the freezing of NaCl solutions. In *Physics of Snow and Ice. Proceedings of the International Conference on Low Temperature Science*, pp. 579–597.
- WETTLAUFER, J. S. 2019 Surface phase transitions in ice: from fundamental interactions to applications. *Phil. Trans. Roy. Soc. A* **377**, 20180261.
- WETTLAUFER, J. S. & WORSTER, M. G. 2006 Premelting dynamics. *Ann. Rev. Fluid Mech.* **38**, 427–452.
- WOLLKIND, D. J. & SEGEL, L. A. 1970 A nonlinear stability analysis of the freezing of a dilute binary alloy. *Philosophical Transactions of the Royal Society of London. Series A* **268**, 351–380.
- WORSTER, M. G. 1986 Solidification of an alloy from a cooled boundary. *Journal of Fluid Mechanics* **167**, 481–501.
- WORSTER, M. G. & WETTLAUFER, J. S. 1999 The fluid mechanics of premelted liquid films. In *Fluid Dynamics at Interfaces*, pp. 339–351. Cambridge, UK: Cambridge University Press.
- XU, Z., YU, H., YAN, J. & TAN, L. 2016 Solidification of suspended colloids at nonplanar interfaces. *Macromolecular Symposium* **365**, 17–31.
- YOU, J., WANG, J., WANG, L., WANG, Z., LIA, J. & LIN, X. 2018*a* In situ observation of the unstable lens growth in freezing colloidal suspensions. *Colloids and Surfaces A: Physicochemical and Engineering Aspects* **553**, 681–688.
- YOU, J., WANG, Z. & WORSTER, M. G. 2018*b* Controls on microstructural features during solidification of colloidal suspensions. *Acta Materialia* **157**, 288 – 297.